Applied Mathematical Modelling 34 (2010) 266–283

Contents lists available at ScienceDirect

Applied Mathematical Modelling

journal homepage: www.elsevier.com/locate/apm

Elastoplastic deformation during projectile–wall collision

Paul W. Cleary *

CSIRO Mathematical and Information Sciences, Private Bag 33, Clayton South, Vic 3169, Australia

ARTICLE INFO

Article history:
Received 16 March 2008
Received in revised form 5 April 2009
Accepted 21 April 2009
Available online 3 May 2009

Keywords:
SPH
Elastic deformation
Plasticity
von Mises
Impact

ABSTRACT

The Smoothed Particle Hydrodynamics method for elastic solid deformation is modified to include von Mises plasticity with linear isotropic hardening and is then used to investigate high speed collisions of elastic and elastoplastic bodies. The Lagrangian mesh-free nature of SPH makes is very well suited to these extreme deformation problems eliminating issues relating to poor element quality at high strains that limits finite element usage for these types of problems. It demonstrates excellent numerical stability at very high strains (of more than 200%). SPH can naturally track history dependent material properties such as the cumulative plastic strain and the degree of work hardening produced by its strain history. The high speed collisions modelled here demonstrate that the method can cope easily with collisions of multiple bodies and can also naturally resolve self-collisions of bodies undergoing high levels of plastic strain. The nature and the extent of the elastic and plastic deformation of a rectangular body impacting on an elastic wall and of an elastic projectile impacting on a thin elastic wall are investigated. The final plastically deformed shapes of the projectile and wall are compared for a range of material properties and the evolution of the maximum plastic strain throughout each collision and the coefficient of restitution are used to make quantitative comparisons. Both the elastoplastic projectile–elastic wall and the elastic projectile–elastoplastic wall type collisions have two distinct plastic flow regimes that create complex relationships between the yield stress and the responses of the solid bodies.

1. Introduction

Smoothed Particle Hydrodynamics is a mesh-free or particle based Lagrangian method for solving systems of partial differential equations. Material is spatially discretised as SPH 'particles' using the SPH interpolation process and governing partial differential equations are converted to rates of change of state variables stored on the particles. Critically the solution is solved on these particles, which move with the material flow, rather than using any fixed mesh or grid structure. Hence the method is both Lagrangian and mesh-free. Originally developed for astrophysical applications by Gingold and Monaghan [1], it was later extended to solve the Navier–Stokes equations for the flow of incompressible fluids by Monaghan [2]. The method has subsequently been used extensively to predict free surface and industrial fluid flows (see [3,4] for many examples) and for many astrophysical applications (see [3]).

The earliest modelling of elastic solids using SPH was by Libersky [5] and then [6]. Gray et al. [7] presented an extension of this early work including a method for overcoming the tensile instability that otherwise leads to numerical fracture. Over the past several years the method has also been adopted for solving problems involving extreme solid deformation, including modelling of industrial forming processes such as extrusion and forging and [8,9]. Liu [10] compared SPH and FEM predictions for the case of moderate amplitude elastoplastic deformation during high speed collision of a cylindrical bar with a

* Tel.: +61 3 9545 8005; fax: +61 3 9545 8080.
E-mail address: paul.cleary@csiro.au

0307-904X/$ - see front matter © 2009 Elsevier Inc. All rights reserved.
doi:10.1016/j.apm.2009.04.004

perfectly reflecting solid (the Taylor problem) and obtained good agreement. Recently, Das and Cleary [11] have systematically evaluated the accuracy, stability and convergence of SPH for elastic solid deformation, including both short term stress wave propagation and long term uniform state response for uniaxial comperall, the SPH method produces very similar performance to the finite element method to which is was compared, but does not suffer from the known problems relating to poor element shape under high deformations.

Using only particles with no prescribed geometric linkages (such as in a mesh or a grid) allows high solid deformations to be dealt with easily in cases where finite element methods would either fail and/or require expensive and diffusive re-meshing. SPH is also able to predict complex surface deformation, including fragmentation without the need for any explicit surface tracking methods. Another advantage of SPH for solid deformation systems is its natural ability to track material history. Each SPH particle represents a specific volume of material, which can have different properties to other particles. These properties can be dependent on the flow history, such as the stress or strain, microstructure and composition.

In this paper, the SPH method for elastic solid deformation is modified to include von Mises plasticity with linear isotropic hardening. It is then used to investigate high speed collisions of an elastoplastic projectile with a thin elastic wall and between an elastic projectile and a thin elastoplastic wall. The dependence of the coefficient of restitution and the final shape of the plastically deformed body on the yield stress are examined in detail in two dimensions. For each collision scenario two distinct plastic flow regimes are identified and control the development of the plastic strain of the rebound of the projectile.

2. SPH method for solid deformation

2.1. Elastic solid governing equations

Following [3] the interpolated value of a function A and its derivative at any position $\mathbf{r}$ can be expressed using SPH smoothing as:

$$A(\mathbf{r}) = \sum_b m_b \frac{A_b}{\rho_b} W(\mathbf{r} - \mathbf{r}_b, h) \tag{1}$$

and

$$\nabla A(\mathbf{r}) = \sum_b m_b \frac{A_b}{\rho_b} \nabla W(\mathbf{r} - \mathbf{r}_b, h), \tag{2}$$

where m_b and $\mathbf{r}_b$ are the mass and density of particle b and the sum is over all particles b within a radius 2 h of $\mathbf{r}$. Here $W(\mathbf{r},h)$ is a C^2 spline based interpolation or smoothing kernel with radius 2 h, that approximates the shape of a Gaussian function but has compact support. Using these interpolation formulae and suitable finite difference approximations for second order derivatives, one is able to convert parabolic partial differential equations into ordinary differential equations for the motion of the particles and the rates of change of their properties.

The SPH continuity equation [3] is:

$$\frac{d\rho_a}{dt} = \sum_b m_b (\mathbf{v}_a - \mathbf{v}_b) \cdot \nabla W_{ab}, \tag{3}$$

where ρ_a is the density of particle a with velocity $\mathbf{v}_a$ and m_b is the mass of particle b. We denote the position vector from particle b to particle a by $\mathbf{r}_{ab} = \mathbf{r}_a - \mathbf{r}_b$ and let $W_{ab} = W(\mathbf{r}_{ab},h)$ be the interpolation kernel with smoothing length h evaluated for the distance $|\mathbf{r}_{ab}|$. This form of the continuity equation is Galilean invariant, has good numerical conservation properties and is not affected by free surfaces or density discontinuities.

The governing or flow equation used for elastic and elastoplastic deformation of the solids is:

$$\frac{d\mathbf{v}}{dt} = \frac{1}{\rho} \nabla \cdot \boldsymbol{\sigma} + \mathbf{g}, \tag{4}$$

where $\mathbf{v}$ is velocity, $\mathbf{g}$ denotes the body force and σ is the stress tensor which can be written as:

$$\boldsymbol{\sigma} = -P\mathbf{I} + \mathbf{S}, \tag{5}$$

where P is the pressure, $\mathbf{S}$ is the deviatoric stress, and $\mathbf{I}$ is the identity matrix. We use a neo-Hookian elasticity model with a shear modulus G. The SPH form of Eq. (4) expressed in terms of overall stress is:

$$\frac{d\mathbf{v}_a}{dt} = \sum_b m_b \left(\frac{\boldsymbol{\sigma}_a}{\rho_a^2} + \frac{\boldsymbol{\sigma}_b}{\rho_b^2} + \Pi_{ab}\mathbf{I} \right) \cdot \nabla_a W_{ab} + \mathbf{g}_a \tag{6}$$

where $\boldsymbol{\sigma}_a$ and $\boldsymbol{\sigma}_b$ are the stress tensors of particles a and b, and $\mathbf{g}_a$ is the body force at particle a. Π_{ab} is an artificial viscous stress term with shear and bulk viscosity components and is given by Monaghan [2] as:

$$\begin{aligned} \Pi_{ab} &= \frac{-\alpha c_0 \eta_{ab} + \beta \eta_{ab}^2}{\bar{\rho}_{ab}} \quad \text{if } (\mathbf{v}_a - \mathbf{v}_b) \cdot (\mathbf{r}_a - \mathbf{r}_b) < 0 \\ &= 0 \qquad\qquad\qquad\quad \text{otherwise}, \end{aligned}$$

where

$$\eta_{ab} = \frac{h(\mathbf{v}_a - \mathbf{v}_b)\cdot(\mathbf{r}_a - \mathbf{r}_b)}{|\mathbf{r}_a - \mathbf{r}_b|^2} \quad \text{and} \quad \bar{\rho}_{ab} = \frac{(\rho_a + \rho_b)}{2}.$$

Here $\alpha = 1.0$ and $\beta = 2$ are constants. The linear term of Π_{ab} produces a shear and bulk viscosity, and the quadratic term is approximately equivalent to Von Newmann–Richtmeyer viscosity.

The evolution equation for the deviatoric stress S, given by Gray et al. [7], is:

$$\frac{dS^{ij}}{dt} = 2G\left(\dot{\varepsilon}^{ij} - \frac{1}{3}\delta^{ij}\dot{\varepsilon}^{kk}\right) + S^{ik}\Omega^{jk} + \Omega^{ik}S^{kj}, \tag{7}$$

where the strain rate tensor is:

$$\dot{\varepsilon}^{ij} = \frac{1}{2}\left(\frac{\partial v^i}{\partial x^j} + \frac{\partial v^j}{\partial x^i}\right) \tag{8}$$

and

$$\Omega^{ij} = \frac{1}{2}\left(\frac{\partial v^i}{\partial x^j} - \frac{\partial v^j}{\partial x^i}\right) \tag{9}$$

is the Jaumann rotation tensor. The two rotation terms in Eq. (6) accounts for large rotational effects. The SPH versions of Eqs. (6)–(8) are straight forward to derive.

The SPH is compressible and is therefore able to predict stress or acoustic waves. To do this it uses the equation of state. We use a linear form:

$$P = c_0^2(\rho - \rho_0) \tag{10}$$

to relate density and pressure changes, where ρ_0 is the reference density and c_0 is the speed of sound given by $c_0 = \sqrt{\frac{K}{\rho_0}}$. Here K is the bulk modulus and the Poisson ratio v is given by:

$$v = \frac{(3K/G - 2)}{2(3K/G + 1)}. \tag{11}$$

2.2. Von Mises plasticity with linear isotropic hardening

The radial return plasticity model of [12] is used to model plastic deformation. A trial deviatoric stress S^{ij}_{Tr} is calculated assuming an initial elastic response. The increment of plastic strain is:

$$\Delta\varepsilon^p = \frac{\sigma_{vm} - \sigma_y}{3G + H}, \tag{12}$$

where σ_{vm} is the von Mises stress and σ_y is the current yield stress. The plastic strain is then incremented:

$$\varepsilon^p = \varepsilon^p + \Delta\varepsilon^p. \tag{13}$$

The yield stress increment $\Delta\sigma_y$ at each time step is calculated as:

$$\Delta\sigma_y = H\Delta\varepsilon^p, \tag{14}$$

where H is the hardening modulus. The deviatoric stress S^{ij} at the end of a time step is given by:

$$S^{ij} = r_s S^{ij}_{Tr}, \tag{15}$$

where r_s is the radial scale factor given by:

$$r_s = \frac{\sigma_y}{\sigma_{vm}}. \tag{16}$$

2.3. SPH solution process

The SPH discretisation gives a coupled set of ordinary differential equations that are integrated using a second order Improved Euler predictor–corrector. Firstly Eqs. (7) and (3) are to give the current deviatoric stress and density. The density is then used in Eq. (10) to give the pressure. Any limiting of the deviatoric stress by the plasticity model is then evaluated using Eqs. (12)–(16). The final deviatoric stress and the pressure along with the current velocity are then used in Eq. (6) to calculate the acceleration of the particles. This equation is then integrated along with the kinematic equations to give updated particle positions.

3. Collision configuration

The dimensions of the projectile used throughout this study was 250 mm × 110 mm. The wall with which the projectile collides was set to be vertical and was 40 mm thick and 1.0 m high. The wall was initially straight and uniform. The projectile starts on the right of the wave and moves to the left towards the wall. Fig. 1 shows the initial position of the projectile and the wall. The ends of the wall were made fixed by setting a zero velocity boundary condition for the particles in the very top and bottom rows of the wall. The initial projectile speed was 100 m/s in all cases. The specific choice of projectile and wall dimensions and the initial projectile speed are not important since we vary the yield stress across a wide range to explore the resulting impact behaviours. Different choices of the geometry and speed simply change the specific values of the yield stress where the observed behaviours occur. The elastic material properties used are given in Table 1. These are reasonable generic values for metallic solids. Since the elasticity of such materials does not vary substantially and the elastic impact problem is not particularly interesting, we use the same elastic properties throughout and concentrate on the effect of the plasticity. The plasticity model has two parameters, these being the yield stress Y and the hardening modulus H. The effect of changing these plasticity parameters is explored in this paper and the values used are quoted in the relevant sections.

The SPH resolution used was 10 mm, giving 925 particles in these two dimensional simulations. They were all run on a 667 MHz single processor alpha workstation. The 15 ms duration simulations took 3 min of cpu time whilst the largest simulations of 100 ms took 20 min. On current single core Intel cpu's the compute time would be around 5 times shorter. These impact related deformation problems are very fast when computed with SPH and three dimensional simulations are also quite feasible.

4. Collision of elastoplastic projectile with an elastic wall

Firstly, we examine the collision of an elastoplastic projectile with an elastic wall.

4.1. Perfectly plastic material

Fig. 2 shows the elastoplastic deformation of a relatively hard perfectly plastic (meaning $H = 0$) rectangular projectile (moving to the left) impacting on the thin elastic wall. The SPH particles are shaded by their amount of plastic strain. Light grey (as seen on the right of the projectile and for the wall) corresponds to zero plastic strain. Near black corresponds to the highest plastic strain at that time. Note that the peak plastic strain increases with time. Upon initial contact with the wall, the center of the wall bows to the left slightly. Modest plastic deformation is observed in the projectile near the wall with the high levels observed at its corners where these stresses are highest.

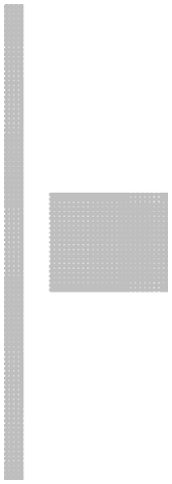

Fig. 1. Collision configuration with a thin vertical wall on the left and a projectile on the right moving towards the wall.

Table 1
Elastic properties of the projectile and wall.

Object	Bulk modulus K (Pa)	Shear modulus G (Pa)
Projectile	1.22×10^{10}	2.67×10^{7}
Wall	1.22×10^{10}	2.67×10^{9}

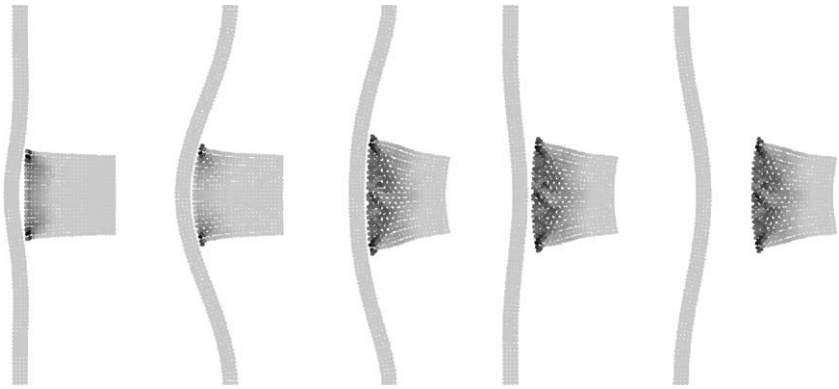

Fig. 2. Elastoplastic deformation of a relatively hard (Y = 5 MPa) rectangular projectile (moving to the left) impacting a thin elastic wall.

In the next frame, the projectile has moved to the left and the entire length of the wall is now bowed out with the largest deformation at its center. The deformation of the wall in this case is purely elastic. The projectile is slowed as energy is dissipated in the plastic deformation of the projectile and stored in the elastic deformation of the wall. The leading surface is deformed both elastically and plastically to conform to the shape of the inner surface of the wall with which it is colliding. The plastic strain at the corners has increased and narrow protrusions can be observed at the leading corners of the projectile. The majority of the projectile is either not deformed or is mildly elastically deformed. The plastic deformation remains both mild and concentrated near the contact surface.

Between the second and third frames, the wall reaches its maximum deformation and the forward progress of the projectile ceases. The elastically loaded wall then begins to unload and starts to accelerate back towards the projectile. In the third frame (Fig. 2) the returning wall (now moving to the right) applies very high stresses across the entire contact face of the projectile leading to rapid plastic failure of a triangular zone starting at the projectile corners and reaching to a almost to the center of the projectile. More moderate plastic deformation is observed along the side of just over half the length of the projectile. The material to the right of this does not undergo plastic deformation. The very high compressive forces generated by the wall and projectile moving in opposite directions rapidly leads to the projectile ceasing forward motion and being accelerated backwards. The elastic unloading of the wall continues to accelerate the projectile to the right but once the wall and projectile are moving in the same direction again, the stresses decline substantially and only very modest increases in the plastic deformation are observed. In the fourth frame the middle of the wall has moved to the right of its initial position but is now decelerating. The projectile therefore separates from the wall and moves to the right. No further change is observed in the projectile. The final shape is essentially trapezoidal with slightly curved leading and trailing edges and slight protrusions at the corners of the rear (collision) face. The plastic deformation increases with proximity to the rear face.

The plastic flow during this collision has two regimes:

1. There is only small plastic deformation after initial as the elastic wall is loaded. The wall rapidly reaches the same speed as the projectile leading to relatively low compressive stress and limiting the plastic deformation whilst the two bodies move together.
2. Once the elastic wall has reached its maximum extension it changes directions and accelerates rapidly back in the other direction. The combination of this rapid return movement to the right with the residual movement of the projectile to the left generates a significant increase in the compressive stress in the projectile leading to broad and rapid plastic failure on the left side of the projectile. These stresses are focused in a triangular region where the highest plastic strains are observed. Once the projectile has accelerated back to the same speed as the wall, the stresses drop sharply and plastic deformation ceases.

Fig. 3 shows the elastoplastic deformation of a softer rectangular projectile impacting on the thin elastic wall. Light grey again shows material with no plastic strain and dark grey shows the maximum current plastic strain. Upon initial contact with the wall (second frame), there is again some initial plastic deformation at the leading edge of the projectile with peak deformation of 23% occurring at its corners. As the projectile pushes further against the wall and the wall bows to the left (third frame), the plastic failure extends into the projectile in a triangular zone from the corners. Small protrusions are formed at the corners of the projectile. The peak strain has now reached 60%. In the fourth frame the wall has now reached its maximum extension and has started moving back to the right. The wall and the projectile are now moving in opposite directions and the compressive stresses in the projectile rise sharply. Significant plastic deformation now occurs at the front of the projectile with significant transverse flow of material along the wall. The peak strain has now reached 90%. The returning wall accelerates to the right and the rate of deformation increases leading to a significant flattening of the projectile and a near doubling of its width with peak strains reaching 155% at the time of separation from the wall. As the middle of the wall moves to the right its initial position it applies higher stresses along the middle of the projectile leading to a bending of the

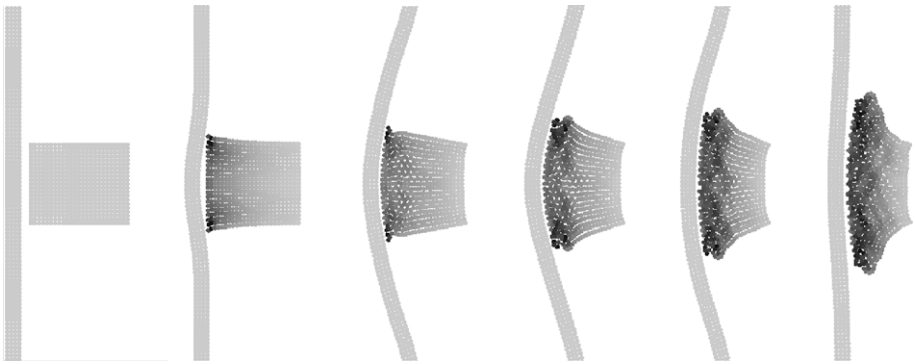

Fig. 3. Elastoplastic deformation of a softer ($Y = 0.1$ MPa) rectangular projectile (moving to the left) impacting a thin elastic wall.

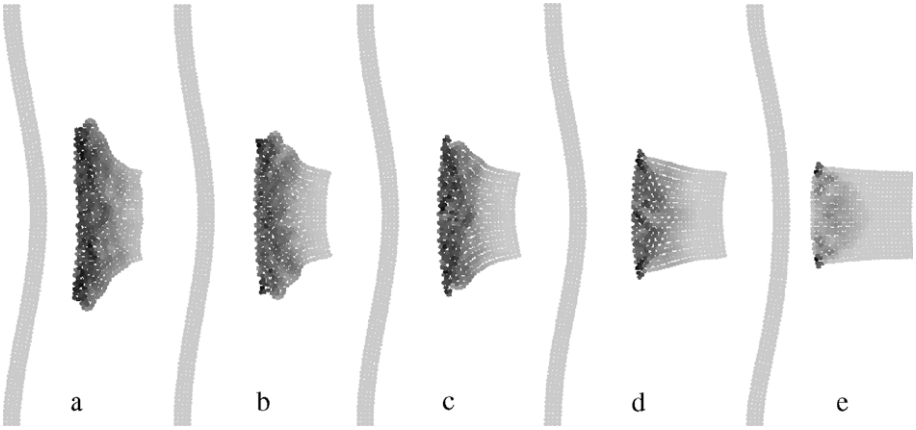

Fig. 4. Final shape of elastoplastic projectiles after collision for different yield stresses: (a) $Y = 10^5$, (b) $Y = 10^6$, (c) $Y = 2 \times 10^6$, (d) $Y = 5 \times 10^6$ and (e) $Y = 10^7$.

flattened body. The final shape after separation from the wall is shown in Fig. 4a. The original corners of the projectile can still be seen. The right edge is almost straight again but the left edge has a modest curvature reflecting the curvature of the wall at the time when the bodies separated. The projectile has its maximum transverse deformation, the form of circular protrusions, about 25% of the way from the left to the right. This is in contrast to the previous higher yield strength material where the peak deformation occurred at the corners.

Fig. 4 shows the final shape of elastoplastic projectiles after collision for different yield stresses. The softest of the materials with $Y = 10^5$ (Fig. 4a) has just been discussed and produces the largest plastic deformations and the largest shape change with significant flattening and bending of the body. For $Y = 10^6$ (Fig. 4b) there is still significant plastic deformation and the structural changes are similar to the previous softer material, but just less extreme. The shape is broadly similar, just less flattened. The largest difference is the reduced plastic deformation in the last 25% of the original projectiles length. For $Y = 2 \times 10^6$ (Fig. 4c) the final shape is more different. More of the right of the projectile is undeformed and the circular protrusions from the sides near the collision edge are now less prominent than the sharp protrusions generated at the corners on the left of the projectile. The body is now almost trapezoidal in shape. Fig. 4d shows the final shape for $Y = 5 \times 10^6$. This is the case whose deformation process is shown in Fig. 2. The shape is modestly trapezoidal with the high deformation occurring only in a triangular failure region starting from the left corners. Small protrusions are visible at the corners and there is now no sign of the circular protrusions on the top and bottom surfaces observed for the lower yield stresses. For $Y = 10^7$ (Fig. 4e) the amount of plastic deformation is quite small, being restricted to a triangular region connecting the left corners and the geometric center of the projectile. Again small sharp protrusions have been created at the left corners where the highest plastic strains are observed. For $Y > 2 \times 10^7$ no plastic deformation is observed for this collision arrangement.

Fig. 5 shows the change in the maximum plastic strain throughout the collision process for a broad range of yield stresses. For $Y = 2 \times 10^7$ the peak plastic deformation is only 5% and is observed at just the left corners which are gently deformed outwards. For higher yield stresses the behaviour is entirely elastic as the compressive stresses generated by the collision do not reach the yield stress. At the other end of the range, we see very little difference between the plastic evolution histories for $Y = 10^4$ and 10^5. This is the perfectly plastic limit where the deformation behaviour becomes independent of the yield stress. The yield stress in Eq. (11) becomes small compared to von Mises stress and so the plastic strain increments become independent of the yield stress and almost all stresses in the material cause plastic deformation. This is the perfectly

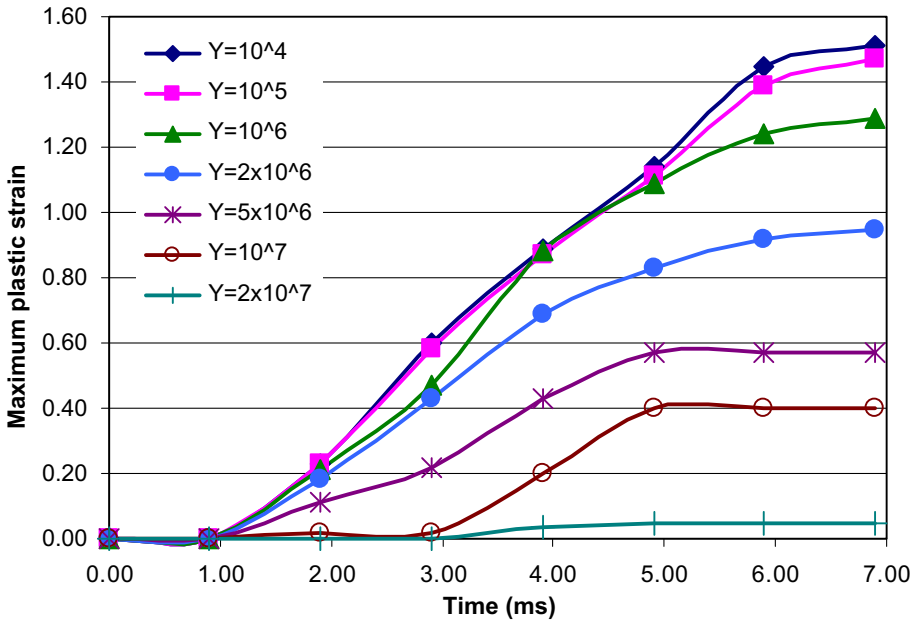

Fig. 5. Change in the maximum plastic strain in the projectile during the collision process for different yield stresses (in Pa) with no hardening.

plastic limit. This demonstrates that the SPH prediction of elastoplastic behaviour is naturally able to recover both the elastic and perfectly plastic limits of behaviour.

Between these two limits, the plastic strain evolution changes monotonically with increasing yield stress leading to higher levels of plastic strain at each time. The levels of yield stress are roughly spaced by factors of two. The final plastic strain levels increase monotonically with yield stress but are not entirely linear (as shown by the modestly uneven spacing of the curves). The plastic strain evolution curves have a number of stages. Initial contact occurs just before 1 ms, so there is no plastic strain before this. Between 1 ms and 3 ms corresponds the first of the plastic deformation regimes identified above. This occurs as the wall is accelerated to the same speed as the projectile. Since the wall and projectile are moving in the same direction the compressive stresses are comparatively modest and so the plastic deformation rate is lower than experienced later. For the harder materials the deformation from this first regime are very small. By 3 ms, the elastic wall has reached its maximum extension and accelerates rapidly back towards the projectile. This is the second plastic flow regime and produces much higher rates of plastic deformation. This can be seen by the change in gradient of the plastic strain curves at 3 ms. The change in plastic strain rate is between regimes is most pronounced for the higher yield stress materials ($Y \geqslant 5 \times 10^6$). For the softer materials plastic strain occurs more evenly. For the perfectly plastic behaving materials ($Y \leqslant 10^5$) there is little observable difference in the plastic strain rates between flow regimes.

The specific values of the transitions from perfectly plastic to elastoplastic to elastic will depend on the details of the collision configuration. Higher projectile speeds will increase the yield stress thresholds and lower collision speeds will reduce the yield stress thresholds. The two plastic flow regimes, the transition between them and the critical influence of the elastic loading and unloading of the wall are generic to this class of projectile–wall collisions, but the specific yield stresses at which they occur will be collision speed, wall thickness and projectile mass dependent.

The coefficient of restitution for collision is defined here as the ratio of the post-collisional speed to the pre-collision speed of the projectile. Fig. 6 shows the variation of the coefficient of restitution for collision with an elastoplastic projectile with a thin elastic wall as a function of the yield stress of the material. It varies between 0.58 and 0.75 for the full range of elastoplastic behaviour. This is a relatively small range which might surprise some. The contribution of the elastic wall is critical to determining the rebound speed of the projectile. Some may anticipate that the coefficient of restitution should be 1.0 for perfectly elastic cases, but this is not true. The wall is initially deformed to the left, reaches a maximum extension (dependent on the initial kinetic energy of the projectile) and then deforms to the right. At the time of separation the middle of the wall is travelling at the same speed as the projectile. This means that there is significant residual kinetic energy in the wall post collision and the wall oscillates back and forward. So not all the original kinetic energy is returned to the projectile and the coefficient of restitution must be less than 1.0 even for non-dissipative cases. The transfer of energy and momentum to the wall is a key non-dissipative loss mechanism for the projectile. Making simplifying assumptions of half the wall moving at the projectile speed and based on the relative masses of the wall and projectile, we would estimate an upper limit on the coefficient of restitution for the elastic case of 0.85. This is close to the 0.75 value observed.

Elastic energy storage in the wall during collision also strongly influences the lower limit of the coefficient of restitution. Much of the initial kinetic energy of the projectile is transferred to the wall and stored as elastic energy. As the wall unloads

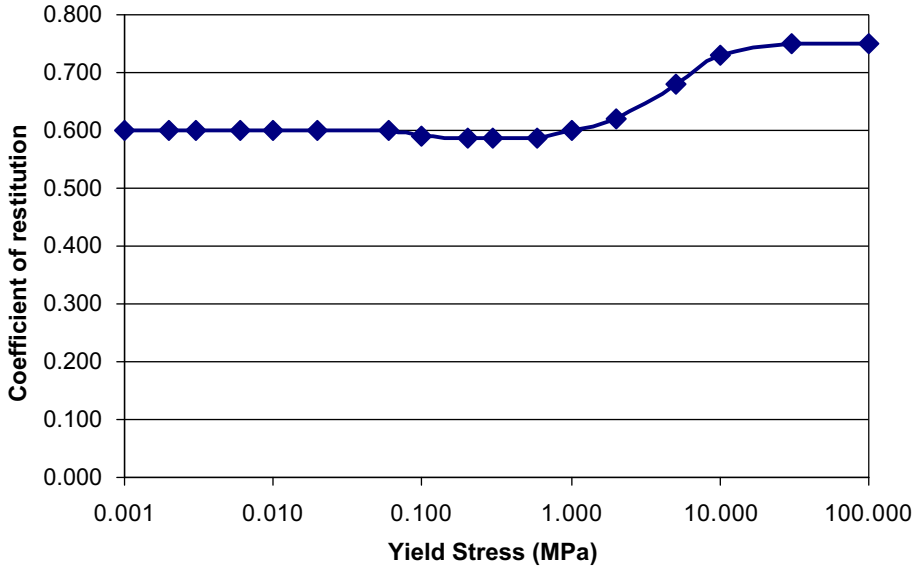

Fig. 6. Coefficient of restitution for collision with an elastoplastic projectile with a thin elastic wall as a function of the yield stress of the material.

and accelerates back to the right much of this energy is returned as kinetic energy to the projectile while some is dissipated by the plastic deformation produced by the internal stresses generated by the acceleration of the projectile by the wall.

For yield stresses below 10 MPa the amount of plastic deformation increases strongly as does the accompanying dissipation. The minimum coefficient of restitution of 0.58 first is attained at a yield stress of 0.6 MPa. The coefficient of restitution decreases approximately linearly in this range. The plastic deformation at 0.6 MPa accounts for dissipating about 22% of the initial kinetic energy. The coefficient of restitution is essentially independent of the yield stresses when it is <0.6 MPa. There is a small elastic effect between 0.1 and 0.6 MPa relating to some residual elastic loading of the projectile upon detachment from the wall. In these cases the projectile does move at constant speed. The parts of the projectile around its mid-plane move slightly faster than the parts of the projectile further out reflecting the non-uniform speed of the adjacent wall. There is some storage of elastic energy in the projectile as well. This energy dissipates via further plastic work as the velocity equalises some time after the detachment of the projectile from the wall. For the perfectly plastic cases ($Y < 0.1$ MPa) there is very little storage of elastic energy in the projectile and all the energy transferred from the wall manifests as kinetic energy. This means that the post-collision kinetic energy is slightly higher for the perfectly plastic projectiles than it is for the strongly plastic but slightly elastic ones. This is the reason for the small increase in the coefficient of restitution from around 0.58 to 0.6 for the perfectly plastic projectiles.

For the perfectly plastic projectiles ($Y < 10^5$) the shape of the projectile, the maximum plastic strain and the coefficient of restitution all become independent of yield stress.

4.2. Isotropic strain hardening material

Next we investigate the effect of isotropic work hardening of the projectile material during the collision. The transient evolution of the shape is not substantially different to those shown for the different constant yield stresses so we concentrate our analysis on the final shape of the projectile. Fig. 7 shows the final shape of the elastoplastic projectiles after collision for varying levels of isotropic hardening. We choose a base case of an initial yield stress $Y = 10^6$. Fig. 7a shows the final projectile shape when there is no hardening. This is a familiar shape previously shown and discussed in Fig. 4b. For a hardening modulus of 2 MPa, we observe a moderate change in shape. The extent of plastic deformation is reduced, with less flattening and with small circular protrusions from the top and bottom surfaces. For a hardening modulus of 4 MPa, the shape change continues with again reduced flattening and reductions in the size of the circulation protrusions which are not the same size as the sharp protrusions at the corners on the left. A further increase in the hardening modulus to 8 MPa continues the trend with a further mild reduction in the flattening and further reductions in the circular protrusions. In all four cases, the distribution of the plastic strain throughout the projectile is similar. The changes produced are quite similar to those observed when increasing the initial yield stress (shown in Fig. 4). The hardening does not produce any radical changes in behaviour.

Fig. 8 shows the evolution of the maximum plastic strain in the projectile during the collision process for the different levels of isotropic hardening. The non-hardening case has the highest plastic strain at all times. Increasing the hardening modulus monotonically reduces the plastic strain at each time. For $H = 8$ MPa, the plastic strain has been reduced by 50% compared to the non-hardening case. Note that the shapes of the plastic strain curves change shape with increasing hardening. They are not simply being scaled down. The gradients of the strain rate are fairly similar over the first 3 ms, but

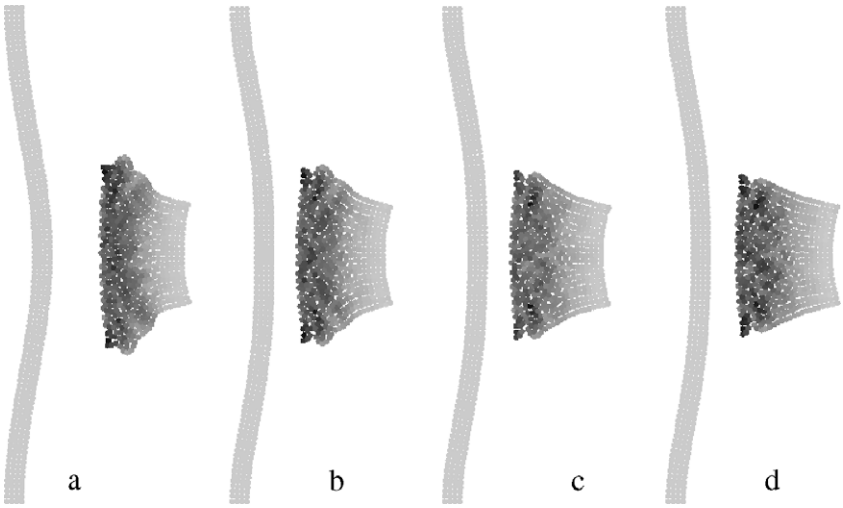

Fig. 7. Final shape of elastoplastic projectiles after collision for varying levels of isotropic hardening (all with the same initial yield stress of 10^6): (a) $H = 0.0$, (b) $H = 2 \times 10^6$, (c) $H = 4 \times 10^6$ and (d) $H = 8 \times 10^6$.

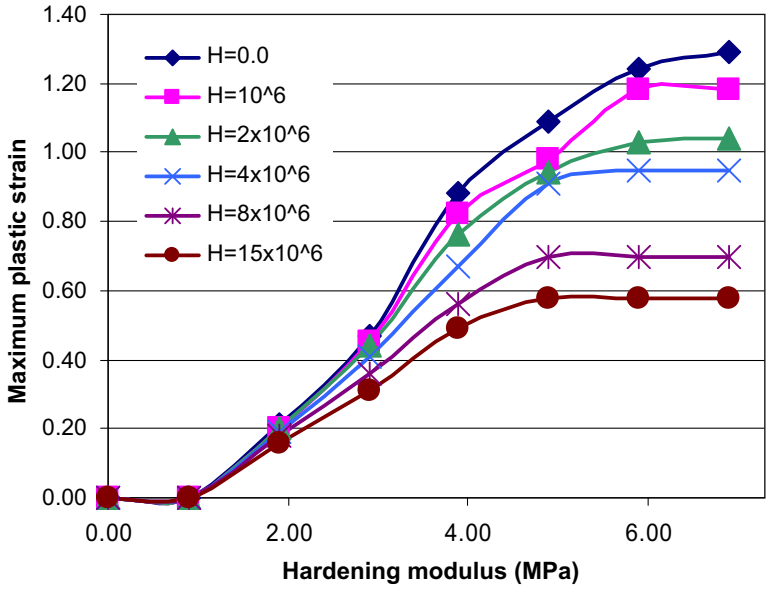

Fig. 8. Change in the maximum plastic strain in the projectile during the collision process for a yield stress of $Y = 10^6$ and varying degrees of isotropic hardening.

increasingly diverge during the second plastic flow regime. The time at which the plastic strain reaches a limit decreases with increasing hardening. This reflects the inability of the stresses late in the collision process to reach the elevated work hardened yield stress produced by the early plastic deformation.

It is useful to compare the non-hardening $Y = 2 \times 10^6$ case (Fig. 4c) with the hardening cases of $Y = 10^6$ (Fig. 7) to see which one matches the behaviour most closely. The best match based on final projectile shape was found for $H = 4 \times 10^6$ (Fig. 7c). Comparing the plastic strain evolution curves from Figs. 5 and 8, we see that these curves are also quite a good match having the same final maximum plastic strain of 0.95. For the hardening case this strain gives a final yield stress for the material of around 4.8×10^6. The average yield stress over this collision is around 2.4×10^6 which is fairly similar to the non-hardening yield stress $Y = 2 \times 10^6$ that was found to most closely match the collision behaviour. This means that the final collision outcomes (projectile shape and maximum plastic strain) are similar for a hardening case to a non-hardening case when the average hardening yield stress is about the same the constant yield stress. The cases are not fully equivalent since the hardening material is initially softer but then harder later. This means that the timing of the deformations is

different with larger deformations earlier and smaller ones later. This is reflected in the somewhat different shapes to the maximum plastic strain curves in Figs. 5 and 8.

4.3. Effect of orientation and rotation on collision behaviour

Fig. 9 shows the initial and final shapes of an elastoplastic projectile after collision for three different projectile orientation; (a) 0°, (b) 14°, and (c) 45°. The collision and deformation processes are essentially the same as for the head-on impact. The two stages of plastic deformation with projectile deforming the wall and then the compression stage produced by the wall accelerating to the right while elastically unloading are similar. The extent of transverse deformation for the angled cases is similar, but the final shape obviously different reflecting the different distribution of material in the body. This is most visible on the right side of the projectile where there is less plastic deformation and the projectile retains identifiable attributes of the original rectangular shape. The details of the transverse plastic deformation near the elastic wall are fairly strongly dependent on the distribution of material around these locations leading to significant variation in the final shape on the left side of the projectile.

Fig. 10 shows collision of a soft elastoplastic projectile that is spinning rapidly (1000 rad/s). The initial contact is on one of the corners (first frame). This material is deformed and slowed. The projectile rotation bends the projectile bringing the end face of the projectile in contact with the wall (second frame). The deformation of the elastic wall is now not symmetric with greater deformation at the top where the faster moving parts of the projectile are making contact. In the third frame, the

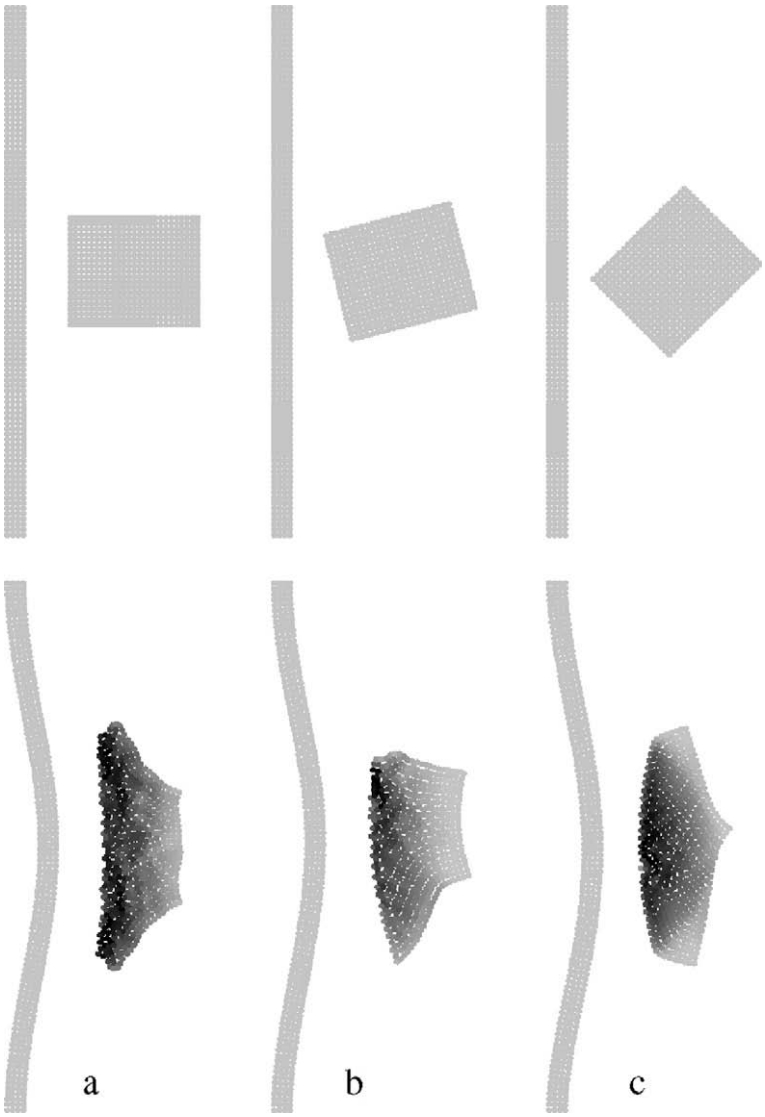

Fig. 9. The initial and final shapes of an elastoplastic projectile after collision for three different projectile orientations: (a) 0° degrees, (b) 14°, and (c) 45°.

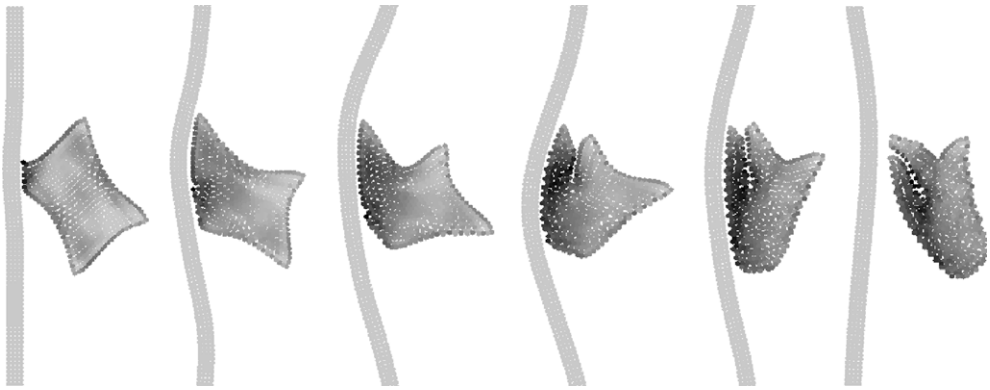

Fig. 10. Extreme elastoplastic deformation of a soft high speed rapidly spinning projectile with an elastic wall.

region in contact with the wall is substantially slowed and is undergoing strong deformation. The initial contact area (that was at one of the original corners) and which was at the bottom of the contact zone with the wall in the previous frame has moved away from the wall. The right half of the body is still rotating around the center of mass of the projectile even though the left hand side is moving much more slowly leading to strong plastic deformation throughout the middle of the body. In the fourth frame, the top left corner of the projectile has continued rotating until it has collided with the material that was previously in the top left corner. The elastic behaviour of the wall is also more complex. At this stage the wall in the upper contact area has already begun moving to the right (the second stronger plastic flow regime) producing significant compression of the upper part of the body and contributing to the folding of the body onto itself and the self collision. In the lower half of the contact area with the wall, is still moving to the left and so the plastic flow is still in the more gentle first plastic flow regime here. In the fifth frame, the entire wall is now moving to the right and significant compression and plastic deformation occurs in the bottom half of the body. This leads to strong flattening of the body parallel to the wall. In the final frame, the fully deformed projectile has separated from the wall. This is an extreme deformation case, where the body has been folded back onto itself and significant plastic deformation has occurred throughout the body. The rebounding body moves directly away from the wall with no rotational component. The plastic deformation has been exceedingly efficient at absorbing the initial rotational kinetic energy of the body. The final shape is highly dependent on the orientation of the body at the contact. Small changes in the initial position and/or the original angle can produce quite different shapes, albeit with similar levels of extreme deformation. SPH has been able to model this type of extreme deformation, including self-collision, without any difficulty or special treatments.

5. Collision of elastic projectile with an elastoplastic wall

Now we study the collision of an elastic projectile with an elastoplastic wall. All other aspects of the configuration are the same as before, we just change the plastic material from the projectile to the wall. This completely changes the collision dynamics. It actually does not matter for the case of an elastoplastic wall if the projectile is elastic or elastoplastic. Since the wall is much thinner than the projectile the stresses are much higher in the wall than in the projectile and essentially all the plastic deformation occurs there.

5.1. First stage plastic deformation

Fig. 11 shows the progress of elastoplastic deformation of a thin wall when impacted by am rectangular elastic projectile. The yield stress of the wall is $Y = 2 \times 10^7$. Upon contact by the projectile, the center section of the wall starts to bow to the left in the region between the corners of the projectile. The von Mises stress rapidly exceeds the yield stress in this region and mild plastic deformation starts to occur. The darker shading shows the areas of plastic strain. The projectile moves to the left (Fig. 11b) and the deformation of the wall increases extending three quarters of the way along the walls to their points of rigid attachment. The highest plastic strain occurs in the regions directly in front of the contact points at the corners of the projectile. Some plastic deformation also occurs at on the right side of the wall about half way from the edges of the projectile and the ends of the wall where the curvature and therefore the tensile stress are highest.

The projectile slows progressively as its kinetic energy is transferred to kinetic and elastic energy of the wall and dissipated in the plastic deformation of the wall. In Fig. 11c, the projectile has stretched the wall so that it has a tri-linear shape. The wall is almost straight and vertical along the contact with the front face of the projectile. The wall extends in straight lines from the corners of the projectile to the fixed end locations. The wall is now loaded and is in moderate tension. High plastic strain is observed in the wall just beside its fixed ends on its right side and in the region adjacent to the corners of the projectile where the stress is most concentrated.

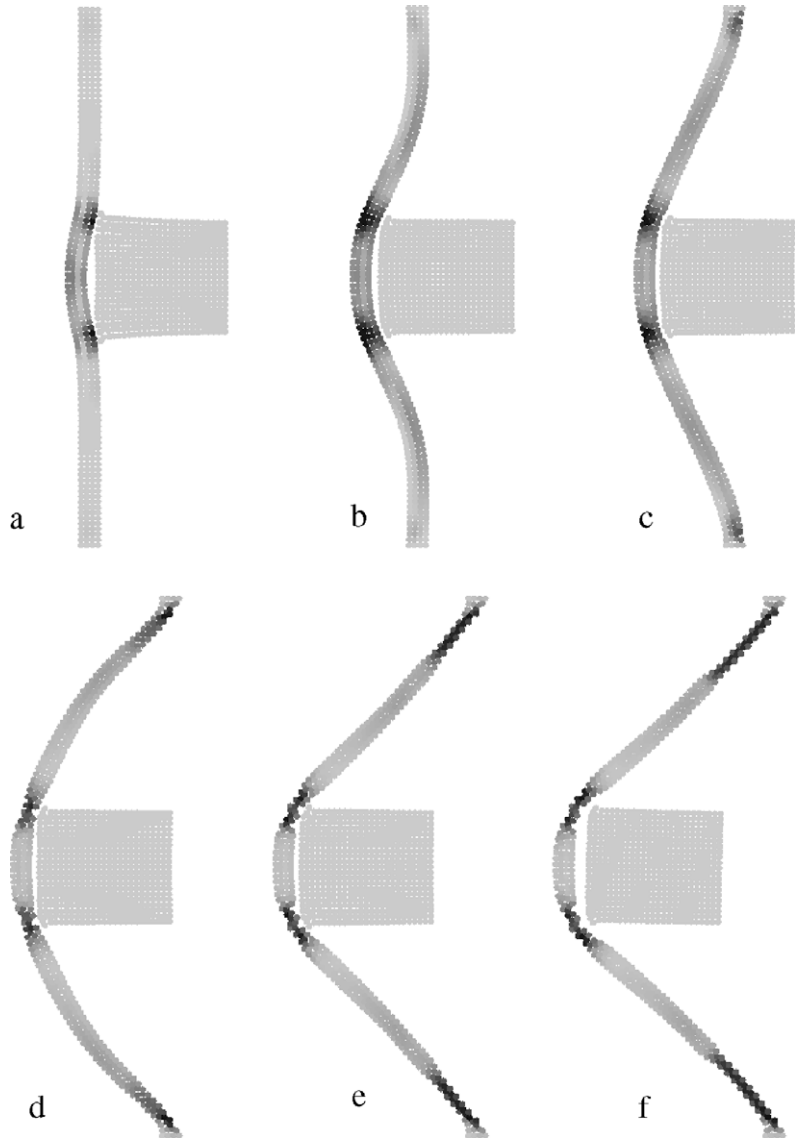

Fig. 11. Progress of elastoplastic deformation of a thin wall when impacted by a rectangular projectile (moving from the right) for $Y = 2 \times 10^7$ with $H = 0$; (a) $t = 1.9$ ms, (b) $t = 2.9$ ms, (c) $t = 3.9$ ms, (d) $t = 5.9$ ms, (e) $t = 7.9$ ms, and (f) $t = 13.9$ ms.

In Fig. 11d, the peak stresses at the contact points with the corners of the projectile and beside the fixed end locations of the wall significantly exceed the yield stress. The material in these regions of high stress concentration stretch rapidly producing ductile necking. This is a behaviour where the material rapidly stretches and thins substantially. The strong plastic failure in these regions relaxes the stresses leading to comparatively low levels of tensile stress in the regions outside the failure zones. Further extension of the wall by the moving projectile causes the stress to rise again. The stress is concentrated at each end of the ductile necking zone leading to plastic failure that propagates along the wall in each direction. Fig. 11e shows ductile necks adjacent to both fixed and ends and at the corners of the projectile. The pattern of increasing stress from the movement of the projectile leading to stress concentration at the end of the plastic failure zones leading to further propagation of the ductile necking failure continues until the kinetic energy of the projectile is exhausted. At this point the stresses fall below the yield stress and no further plastic failure occurs. The residual elastic loading of the wall then unloads accelerating the projectile back to the right. The concentration of the stresses at a few specific locations in the wall leading to plastic failure and stress relaxation prevents the build up of large elastic forces and so the amount of elastic energy stored by the wall is quite low and the projectile rebound is weak. This means that the collision process is highly inelastic and the coefficient of restitution for the collision is small. This is in marked contrast to the earlier case where the rebound of an elastoplastic projectile was found to be reasonably elastic even at very low yield stresses. So the two collision scenarios have radically different behaviour.

Fig. 12 shows the final shape of the wall for four different decreasing yield stresses. Fig. 12a shows the end state for a quite high yield stress. The ductile necking only occurs at the fixture points at the ends of the wall and these zones are quite small. The final deformation of the wall is a bit less than the length of the projectile. As the yield stress declines, the amount of energy dissipated in an increment of plastic deformation of the ductile necking zones decreases. This means that the wall is stretched further and the ductile necking proceeds further to dissipate the kinetic energy of the projectile. In Fig. 12b, the ductile necking at the fixture points has doubled in length and has appeared at the contact points of the corners of the projectile. A further decrease in yield stress doubles the length of all the necked zones and only three small blocks of unstretched wall remain. In the final case for $Y = 5 \times 10^6$, the entire wall has been subject to the propagating ductile necking behaviour and has stretched to more than double its length (and declined to around half its initial thickness) with peak plastic strains of about 150%. The SPH method shows remarkable stability in solving these very high deformation problems even for very thin surfaces.

The process of ductile necking failure propagating along the walls from initial failure points at the fixed wall ends and at the corners of the projectile is the first of two distinct and identifiable plastic deformation regimes for this collision problem. As the yield stress is reduced the ductile necking is increasingly initiated at the corners of the projectile and the failure near the fixed ends is progressively delayed and becomes weaker. This reflects the increasing difficulty of transmitting stress along the walls to its ends as the yield stress declines.

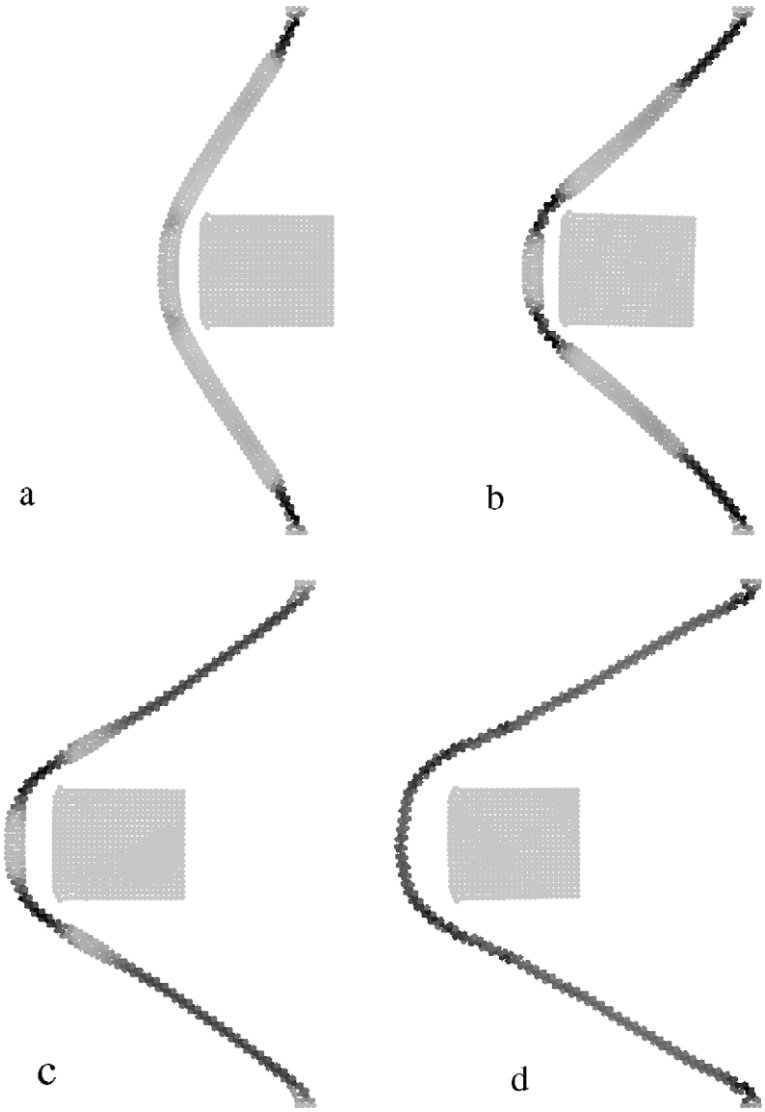

Fig. 12. Final deformed shape of a thin wall when impacted by a rectangular projectile (moving from the right) for different yield stresses, (a) $Y = 5 \times 10^7$, (b) $Y = 2 \times 10^7$, (c) $Y = 10^7$ and (d) $Y = 5 \times 10^6$.

5.2. Second stage plastic deformation

Once the length of the wall has been subject to the ductile necking failure then the first plastic deformation regime is unable to dissipate further energy. So for lower yield stresses the kinetic energy of the projectile is not fully dissipated and a second distinct behaviour is observed. The wall begins to load elastically along its length. The tensile stresses are much more evenly distributed than in the first stage, but there are still regions of higher stress at along the parts of the wall contacting or close to the projectile. The resulting plastic strain is more even than in the first stage and is concentrated most at the corners of the projectile and along the wall that is near the upper and lower edges of the projectile. Fig. 13 shows the progress of elastoplastic deformation of a thin wall when impacted by a rectangular projectile for $Y = 10^6$. Fig. 13a shows state when the first stage ductile necking process is complete. The behaviour leading up to this is the same as shown in Fig. 12. The lower yield stress here means that the projectile is still moving at a reasonable fraction of its initial speed. As mentioned earlier, in this the second stage, the wall extends elastically and also undergoes plastic deformation near the projectile. The shape of the does not change while this stretching occurs. Eventually the projectile comes to rest and all the energy has been transferred to the elastic extension of the wall or dissipated in the second stage plastic deformation.

The unloading process is very interesting and demonstrates the effect of the second stage plastic deformation. The elastically loaded wall begins to unload and contract producing a compressive force on the projectile and starting to accelerate it back to the right. There is little/modest plastic deformation occurring in the wall at this stage and the projectile is elastic so most of elastic strain energy stored in the wall is returned to the projectile as kinetic energy. The projectile accelerates and moves to the right. Fig. 13b shows the state of the system shortly after the projectile has been fully accelerated and has separated from the wall. The unloading wall contracts and moves to the right. The regions that were adjacent to the corners of the projectile act as plastic hinges and the wall bends sharply at right angles. Similar 120° bends occur near the other end of the projectile. These shape preferences for the plastically deformed material reflect the strong stress anisotropy that is frozen into the material in these locations due to the extreme deformation history. In Fig. 13c, the projectile continues to move to the right. The wall to the left of the projectile is moving more slowly than the projectile, but the flat sections between the top pair of plastic hinges and between the bottom ones move vertically in towards the projectile and make strong contact with

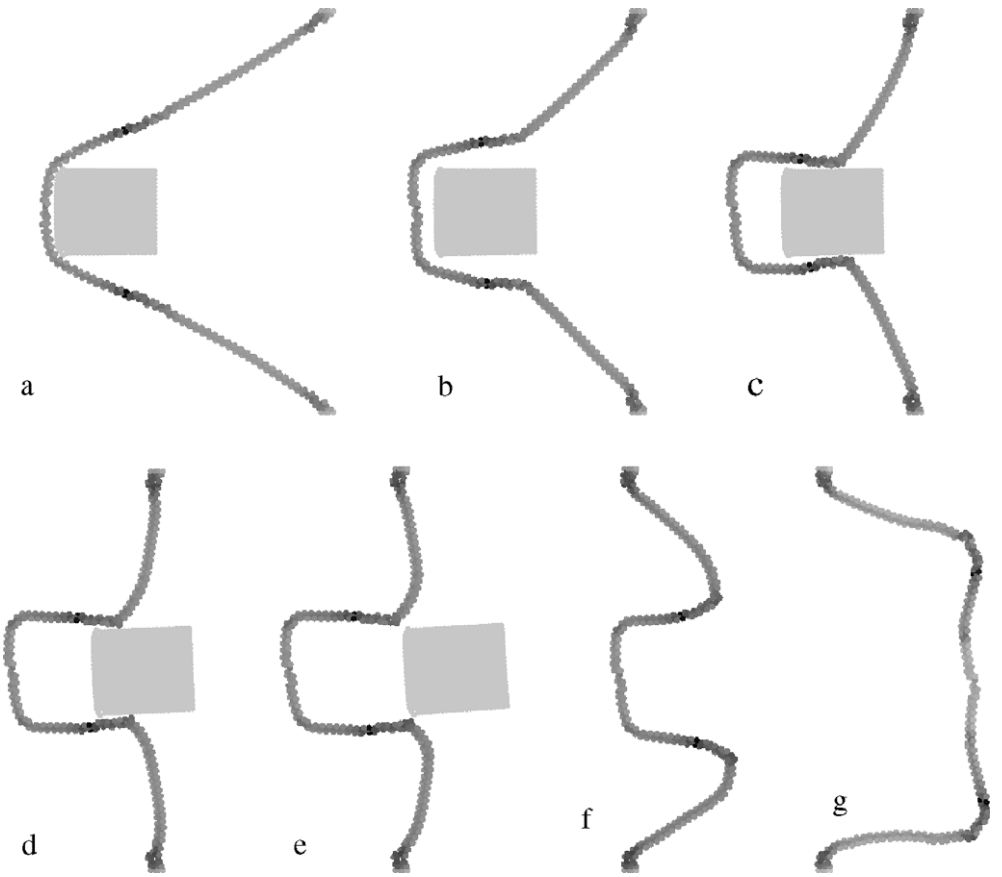

Fig. 13. Progress of elastoplastic deformation of a thin wall when impacted by a rectangular projectile (moving from the right) for $Y = 10^6$ with $H = 0$; (a) $t = 16$ ms, (b) $t = 20$ ms, (c) $t = 24$ ms, (d) $t = 28$ ms, (e) $t = 32$ ms, (f) $t = 44$ ms, and (g) $t = 100$ ms. It demonstrates the first stage ductile necking followed by the elastic loading of the wall and second stage plastic deformation adjacent to the projectile.

its sides. The SPH method is naturally able to detect these additional collisions and to resolve them easily. In Fig. 13d, the projectile has moved further to the right and the wall continues to follow, albeit more slowly. The sections of the wall leading from the fixed ends are not almost vertical. This continues in Fig. 13e with the projectile finally separating from the wall. In the later frames the projectile has moved out of view and is not shown. The central sections of the wall continue to move to the right. This motion generates more plastic deformation near the fixed ends and at the plastic hinges. The central section continues to move to the right slowing as the plastic dissipation consumes its kinetic energy. Eventually the central rectangular region opens back up and becomes almost straight and vertical. The wall sections near the fixed ends are now almost horizontal. In the later stages the deformation is almost entirely plastic and there is little elastic energy stored. So once the configuration shown in Fig. 13g is reached there is no spring-back and this remains as the final shape.

This second stage of plastic deformation is driven by the supply of kinetic energy remaining in the projectile at the end of the first stage. Its complex behaviour is enabled by the large amounts of elastic energy that the already plastically stretched wall is able to store and by the second stage plastic deformation around the projectile that leads to the shape of the projectile being embedded in the plastic strain pattern. There is significant spring-back from the maximally deformed position when the projectile first comes to rest. The elastic unloading of the wall provides significant kinetic energy for both the later wall deformation and for the rapid re-bound of the projectile. The residual kinetic energy of the wall allows the wall shape to change substantially with the plastic deformation concentrated at four plastic hinges and with relatively straight wall sections in between moving fairly rigidly.

This example clearly demonstrates that the SPH method is able to freeze in shape and conformational structure resulting from the plastic deformation history and to retain this embedded shape in later elastic unloading. The complex shape predicted here is somewhat similar to high deformation processes such as deep drawing. Traditional finite element shell mesh models typically need to use complex plasticity models to capture these types of behaviours. This type of deformation behaviour is extreme and may not be possible for many materials. Ductile fracturing could be expected in many conventional metals at different points of the collision and deformation process. This type of extreme deformation without failure is observed in super-plastic forming processes. The remarkable stability of the SPH method for these extreme plastic deformations suggests that SPH may have a role in these sorts of super-plastic forming processes.

5.3. Maximum plastic strain and coefficient of restitution

Fig. 14 shows the change in the maximum plastic strain in the wall during the collision process for a broad range of yield stresses. For wall yield stresses of $Y \geqslant 6 \times 10^8$ there is no plastic deformation. This critical yield stress is much higher than the value of 2×10^7 that was observed when the projectile was elastoplastic. This shows that the stress concentrations in the wall, particularly near the fixed ends, are much higher than the stresses generated in the projectile. These very high stresses also explain why the plastic deformation is localised and once activated is large in scale. The ductile necking failure first occurs near the attachment points of the wall for $Y = 2 \times 10^8$ (open circles in Fig. 14). The plastic strain occurs over a short period soon after the start of the collision after a short period of initial elastic loading. The stress concentration leads to ductile necking in a small region beside the attachment points and this coupled to the elastic energy transfer is enough to stop the

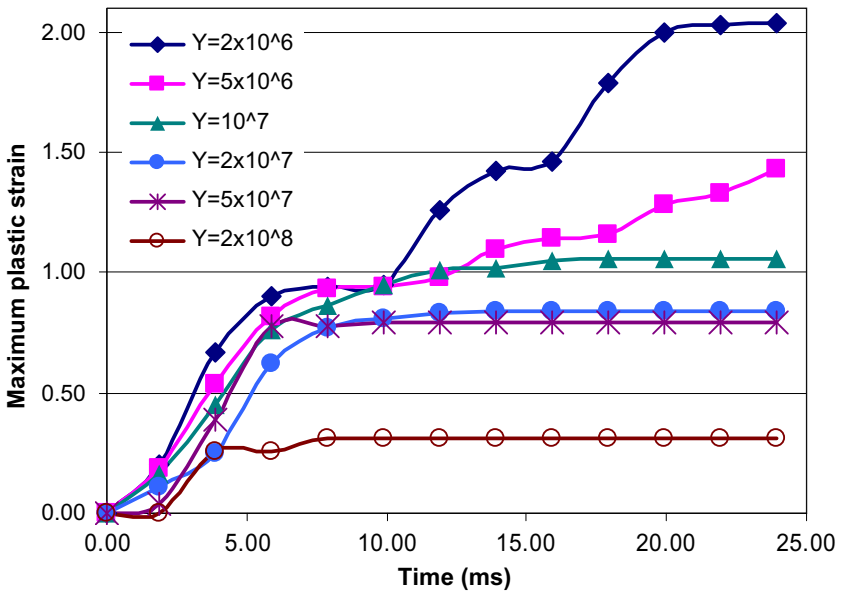

Fig. 14. Change in the maximum plastic strain of the elastoplastic wall during the collision process for different yield stresses (in Pa).

projectile. The stresses remain below the plastic limit after that and the maximum plastic strain remains constant at the initial peak level of 0.31 in the necked region. For $Y = 5 \times 10^7$, the same behaviour is observed but the stress concentration at the end of the current ductile neck starts to propagate along the wall and the length of elongated region increases. The final state for this case is shown in Fig. 12a. The maximum plastic strain therefore starts to rise after the initial elastic loading and continues until the projectile kinetic energy is exhausted. For $Y = 5 \times 10^7$ this occurs at 6 ms and reaches 0.79. Again, once this peak is reached there is no further plastic deformation and the maximum remains constant. Similar behaviour is found for decreasing yield stress down to $Y = 10^7$. Interestingly the maximum plastic strain achieved for all these intermediate yield stresses increase only gradually. The key behaviour is that a small region of wall has a large stress concentration and this leads to localised travelling failure along the wall. The maximum plastic strain in the region is only gently dependent on the yield stress. As the yield stress declines the energy dissipated by a given length of plastic deformation of the wall decreases and so the plastic deformation is forced to continue further along the wall to dissipate sufficient energy to stop the projectile. The means that the time at which plastic deformation ceases and after which the maximum plastic strain is constant in Fig. 14 increases steadily with declining yield stress. This behaviour of a steady increase in maximum plastic stain reaching a plateau part way through the collision is the signature pattern of the first regime of plastic deformation for this collision problem.

For lower yield stresses we enter the second plastic deformation regime during the second half of the collision. The energy dissipation produced by ductile necking of the entire wall is not sufficient to stop the projectile. Now the entire wall becoming elastically loaded and stress concentrations occur over wide areas of the wall that are then subject to a second phase of plastic deformation. This leads to a monotonically increasing maximum plastic strain over the duration of the collision. For $Y = 5 \times 10^6$ the full necking of the wall can be seen in Fig. 12d and the gradient of change in the maximum plastic strain is lower in the second phase of plastic deformation (after 10 ms) than in the initial ductile necking phase. For $Y = 2 \times 10^6$, the maximum plastic strain curve increases in essentially three clearly defined steps. The first step up to 0.95 occurs with this initial ductile necking at the corners of the projectile. The first phase plastic deformation continues steadily until about 10 ms when ductile necking is initiated near the fixed ends of the wall. The necking failure near the walls produces maximum plastic strains of around 1.4 at which time the entire length of the wall has been subject to the ductile necking. The maximum plastic strain remains constant until 16 ms as the wall loads elastically with the projectile ceasing forward motion at 15 ms and then starting to elastically unload. As the projectile and wall accelerate to the right further plastic deformation occurs near the end of wall attachments. This produces the second third step up in the maximum plastic strain to a peak level of 2.04. The forces in the wall then decline and no further increase in plastic strain is observed. Similar behaviours are observed for the softest case $Y = 10^6$ (shown in Fig. 13), but with higher strain levels observed.

Fig. 15 shows the coefficient of restitution for the collision of an elastic projectile with an elastoplastic wall as a function of the yield stress. At very high yield stresses ($Y \geqslant 6 \times 10^8$) there is no plastic deformation and the coefficient of restitution is 0.75 because of non-dissipative transfer of kinetic energy to the wall. The coefficient of restitution drops sharply with decreasing yield stress as a small amount of plastic deformation in the form of ductile necking adjacent to the fixed ends of the walls is sufficient to absorb much of the projectile kinetic energy. For $10^7 < Y < 10^8$ the rate of decrease of the coefficient of restitution is linear but more gradual. This is the range of yield stresses covers the cases shown in Fig. 12 where the

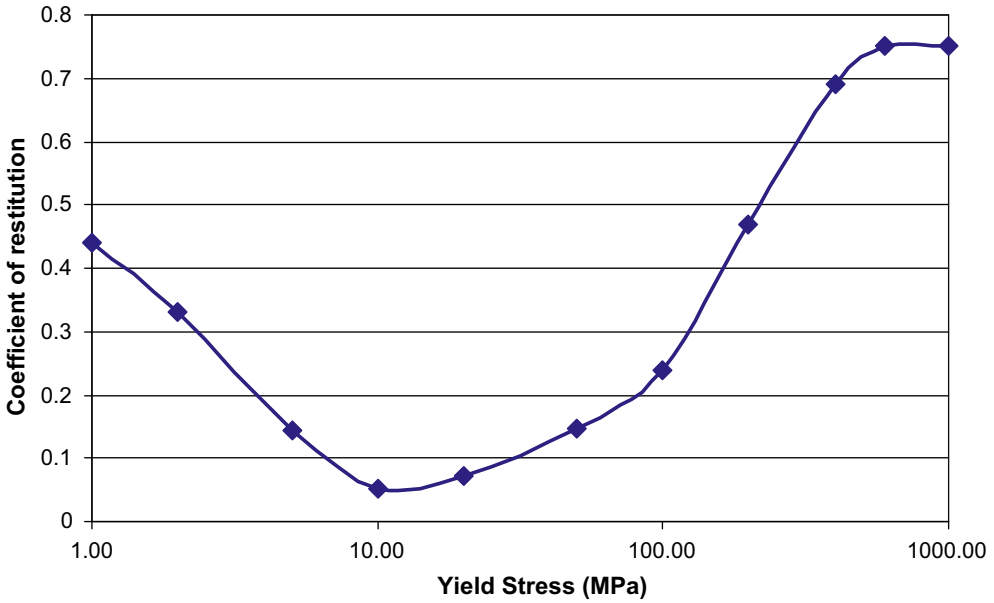

Fig. 15. Coefficient of restitution for collision with an elastoplastic wall as a function of the yield stress of the material.

propagating front of ductile necking travels along the wall from the initiation points dissipating energy. This first phase of plastic deformation produced by the propagating ductile necking is particularly efficient at dissipating kinetic energy and the coefficient of restitution reaches its minimum value of 0.05, making the collisions nearly inelastic.

For lower yield stresses the second phase of plastic deformation takes over with much stronger elastic loading of the wall storing more elastic strain energy that is then returned to the projectile as kinetic energy upon rebound. As the yield stress decreases, the fraction of the initial kinetic energy dissipated in the first phase plastic deformation decreases and increasing projectile kinetic energy remains as the second phase commences. So an increasing fraction of the total energy is stored elastically by the wall and returned as kinetic energy upon rebound, leading to an almost linearly increasing coefficient of restitution. So ironically the softer and more plastic the material is the higher is the coefficient of restitution. The most inelastic behaviour is found at an intermediate yield stress due to the particularly high dissipative efficiency of the ductile necking.

Comparing these results with those for the elastoplastic projectile we find that the plasticity of the wall is much more important in energy dissipation than that of the projectile. Even for much lower yield stresses of the elastoplastic projectile its coefficient of restitution is much higher than when it collides with an elastoplastic wall with a much higher yield stress. The thin wall has a larger area to deform and the thinness of the sheet means that it is effectively less stiff and more easily able to undergo large scale plastic deformation and consequently dissipate more energy. It is also much better at generating very high localised stresses. The location of the peak stress keeps moving with the change in shape of the wall with the necking propagating away from its initiation points.

6. Conclusions

Using a particle method such as SPH with no prescribed geometric linkages (such as in a mesh or a grid) allows very high deformations to be dealt with easily in cases where finite element methods would either fail and/or require expensive and diffusive re-meshing. SPH is also able to predict complex surface behaviour of deforming elastic and elastoplastic solids without the need for any explicit surface tracking methods and can naturally handle cases of multi-body collisions and self-collisions produced by extreme plastic deformation. SPH also has a natural ability to track material history and material property evolution. Each SPH particle represents a specific volume of material, which can have different properties to other particles. These properties can be dependent on the flow history, such as the stress or strain, microstructure and composition.

In this paper, we have explored the elastoplastic collision of a rectangular projectile with a thin wall. The behaviour has been explored for two material combinations where the projectile is elastoplastic and the wall elastic and the second when the projectile is elastic and the wall is elastoplastic. In each case, two flow regimes have been identified. These have been explored in terms of the projectile and wall evolution, their final shape and quantitatively use the time history of the maximum plastic strain and the projectile coefficient of restitution.

For an elastoplastic projectile, the two regimes are:

1. Immediately after the collision starts, there is only a small amount of plastic deformation as the elastic wall is loaded. The wall rapidly reaches the same speed as the projectile leading to relatively low compressive stresses and limiting the plastic deformation whilst the two bodies move together.
2. Once the elastic wall has reached its maximum extension it changes direction and accelerates rapidly back towards the projectile. The combination of this rapid return movement with the residual approach motion of the projectile generates a significant increase in the compressive stress in the projectile leading to broad and rapid plastic failure on the side of the projectile adjacent to the wall. These stresses are focused in a triangular region between the projectile corners and its middle where the highest plastic strains are observed. Once the projectile has accelerated back to the same speed as the wall, the stresses drop sharply and plastic deformation ceases.

The behaviour of this type of collision has been explored for yield stresses that give behaviour ranging from purely elastic to perfectly elastic. In general the plastic strains generated by the first flow regime are lower than in the second with the most extreme difference found for the higher yield stresses and the lowest differences for perfectly plastic materials. The coefficient of restitution of the projectile lies between 0.58 and 0.75 for the full range of yield stresses with the elastic motion of the wall limiting it for both high and low yield stresses. The effect of strain hardening of the projectile during collision has also been explored. A strain hardened material collision behaves in a broadly similar manner to a non-hardening material with a yield stress equal to the average yield stress of the hardening case throughout the collision.

For the collision of an elastic projectile with an elastoplastic wall there are also two regimes of plastic deformation:

1. When the projectile first contacts the wall very high stress concentrations occur at the corners of the projectile and near the attachment points at the ends of the walls. This causes ductile necking in one or more of these regions. As the yield stress declines the energy dissipation of any increment of plastic deformation declines and more plastic deformation is required to halt the projectile. The ductile necking therefore propagates along the walls. This regime is particularly efficient at dissipating energy and the most effectively inelastic collision occurs for the case where almost the entire length of the wall has been stretched in this manner. This produces a minimum coefficient of restitution of 0.05.

2. For materials with lower yield stresses the energy dissipation resulting from the ductile necking of the entire length of the wall is not sufficient to halt the projectile. The second phase of deformation then involves elastic loading of the entire wall length and selective further plastic deformation near the wall attachment points and around the contact surface with the projectile. Once the projectile has been halted, the wall elastically unloads and accelerates both the projectile and wall in the other direction. The wall can undergo further plastic deformation when it loads elastically after moving to full extension in the return direction. The strain levels observed can be extreme (up to 350%) and the shape change in the wall, including indented impressions of the shape of the projectile and the formation of plastic hinges is substantial at lower yield stresses (down to 1 MPa).

The behaviour of this type of collision has also been explored for yield stresses that give behaviour ranging from purely elastic to perfectly elastic. The yield stresses at which the elastic and perfectly plastic behaviour was observed are much higher for the elastoplastic wall than for the elastoplastic projectile reflecting the much lower effective stiffness of the thin wall compared to the thick projectile. The minimum coefficient of restitution was observed at the limit of the first regime of plastic deformation when the ductile necking of the entire wall length is able to dissipate almost all the projectile kinetic energy. For lower yield stresses, the coefficient of restitution rises as the elastic loading of the wall observed during the second regime of deformation stores an increasing fraction of the initial projectile kinetic energy. This gives a complex relationship between wall yield stress and projectile coefficient of restitution.

References

[1] R.A. Gingold, J.J. Monaghan, Smoothed particle hydrodynamics, theory and application to non-spherical stars, Mon. Not. Royal Astron. Soc. 181 (1977) 375–389.
[2] J.J. Monaghan, Smoothed particle hydrodynamic, Annu. Rev. Astron. Astrophys. 30 (1992) 543–574.
[3] J.J. Monaghan, Smoothed particle hydrodynamics, Rep. Prog. Phys. 68 (2005) 1703–1759.
[4] P.W. Cleary, M. Prakash, J. Ha, A.N. Stokes, C. Scott, Smoothed particle hydrodynamics: status and future potential, Prog. Comput. Fluid Dyn. 7 (2007) 70–90.
[5] L.D. Libersky, A.G. Petschek, Smooth particle hydrodynamics with strength of materials, in: S. Trease, M. Crowley (Eds.), Advances in the Free-Lagrange Method, Springer, Berlin, 1990.
[6] C.A. Wingate, H.N. Fisher, Strength Modeling in SPHC. Los Alamos National Laboratory, Report No. LA-UR-93-3942, 1993.
[7] J.P. Gray, J.J. Monaghan, R.P. Swift, SPH elastic dynamics, Comput. Methods Appl. Mech. Eng. 190 (49–50) (2001) 6641–6662.
[8] J. Bonet, S. Kulasegaram, Correction and stabilization of smooth particle hydrodynamics methods with applications in metal forming simulations, Int. J. Numer. Methods Eng. 47 (6) (2000) 1189–1214.
[9] P.W. Cleary, M. Prakash, J. Ha, Novel applications of smoothed particle hydrodynamics (SPH) in metal forming, J. Mater. Process. Technol. 177 (2006) 41–48.
[10] Z.S. Liu, High velocity impact dynamic response of structures using SPH method, Int. J. Comput. Eng. Sci. 5 (2004) 315–326.
[11] R. Das, P.W. Cleary, Simulation of uniaxial compression tests and stress wave propagation using smoothed particle hydrodynamics, Int. J. Numer. Methods Eng., submitted for publication.
[12] J.L. Wilkins, Calculation of Elastic–Plastic Flow, Methods of Computational Physics, vol. 8, Academic Press, New York, 1964. pp. 211–263.